Spin Structure Function Physics with an Upgraded PHENIX Muon Spectrometer

The *PHENIX/Spin* Collaboration

October 27, 1994

Abstract

A major investment by the RIKEN Spin Group makes feasible a significant enhancement of the polarized collider program of the PHENIX Detector using the muon detection capability. The addition of a second muon end cap and muon identification in the central rapidity region yields a detector with large acceptance for high mass muon pairs. The upgrade makes feasible a program of polarized quark and antiquark structure function physics using Drell-Yan continuum and vector boson production. It also adds significantly to the array of measurements feasible for investigating gluon polarization via heavy quark production.

The proposal of the RHIC Spin Collaboration was approved one year ago based on the PHENIX detector of the Conceptual Design Report (CDR). The principal operational difference in the present proposal is a request for polarized proton operating time at $\sqrt{s} = 50\ GeV$. This energy optimizes the rate of high-$\sqrt{\tau}$ Drell-Yan pairs where large polarization effects are most likely to be observed. It also minimizes backgrounds from competing processes, principally semi-leptonic charm decay.

Collaborating Institutions

- PHENIX Collaborating Institutions[1]
  - Bombay Research Institute, *Bombay, India*
  - Brookhaven National Laboratory, *Upton, NY 11973*
  - University of California, Riverside, *Riverside, CA 92521*
  - Chinese Institute of Atomic Energy, *Beijing, China*
  - Chung-ang University, *Seoul, Korea*
  - Columbia University, Nevis Labs., *Irvington, NY 10533*
  - Institute for High Energy Physics, Academia Sinica, *Beijing, China*
  - Institute of High Energy Physics, *Protvino, Russia*
  - Institute of Modern Physics, Academia Sinica, *Lanzhou, China*
  - Institute for Nuclear Research, *Moscow, Russia*
  - Iowa State University, *Ames, IA 50011*
  - Joint Institute for Nuclear Research, *Dubna, Russia*
  - Korea University, *Seoul, Korea*
  - Kurchatov Institute of Atomic Energy, *Moscow, Russia*
  - Lawrence Livermore National Laboratory, *Livermore, CA 94550*
  - Los Alamos National Laboratory, Los Alamos, NM 87545
  - Louisiana State University, *Baton Rouge, LA 70803*
  - Oak Ridge National Laboratory, *Oak Ridge, TN 37831*
  - Peking University, Institute for Heavy-Ion Physics, *Beijing, China*
  - Petersburg Nuclear Physics Institute, *St. Petersburg, Russia*
  - University of Sao Paulo, *Sao Paulo, Brazil*
  - Seoul National University, *Seoul, Korea*
  - Soong-Sil University, *Seoul, Korea*
  - University of Tennessee, *Knoxville, TN 37996*
  - Vanderbilt University, *Nashville, TN 37235*
  - Yonsei University, *Seoul, Korea*

[1] for a full list of the collaboration see the PHENIX home page at http://rsgi01.rhic.bnl.gov/export1/phenix/WWW/phenix_home.html

- New Institutions and Participants
  - Institute for Chemical and Physical Research (RIKEN), *Hirosawa, Wako, Japan*
    T. Ichihara, M. Ishihara,[2] Y. Wantanabe
  - Kyoto University, *Kyoto, Japan*, and RIKEN
    H. Enyo, K. Imai, H. Kaneko, A. Masaike, T. Murakami, M. Yosai
  - Tokyo Institute of Technology, *Tokyo, Japan*, and RIKEN
    T.-A. Shibata
  - New Mexico State University, *Las Cruces, NM*
    G. Kyle

Spokesmen: K. Imai, Kyoto University and RIKEN
J.M. Moss, Los Alamos National Laboratory

Local Coordinators: Y. Makdisi and M.J. Tannenbaum

[2]Also affiliated with the University of Tokyo, Tokyo, Japan

Contents

1 Introduction

1.1 Polarized Structure Function Physics

A major resurgence of interest in the spin structure of the nucleon followed the 1988 publication[1] of small-x measurements of $g_1^p(x)$ by the European Muon Collaboration (EMC). Analysis of the EMC data and larger-x deep-inelastic scattering (DIS) data from SLAC[2] gave rise to the so-called "spin crisis" – the observation that the integral contribution of the up and down quarks to the proton's helicity was small[3].

The past six years has seen an enormous effort to acquire more precise DIS data using polarized electron and muon beams. New measurements of $g_1^p(x)$ confirm[4] the earlier EMC results, and new data on the neutron from DIS on polarized ^2H [5] and polarized ^3He[6] add significantly to our knowledge of quark polarization in the nucleon system. The search for new understanding continues. A major effort is underway at DESY where the HERMES[7] experiment will extend DIS to more exclusive channels. Experiments are also envisioned at SLAC using 50 GeV polarized electrons and at CEBAF exploiting parity violation.

In spite of the large body of new data and the promise of even better experiments in the near future, polarized DIS measurements have major limitations. They do not directly provide any information about antiquark or gluon helicity distributions. Neither can they probe the potentially equally interesting, and completely unknown, chiral-odd quark structure functions[8, 9, 10, 11, 12, 13, 14]; hence the interest in polarized hard-hadronic processes which could offer new physics insight, complimentary to polarized DIS[15, 16].

1.2 The RHIC Spin Collaboration and PHENIX/Spin

The RHIC Spin Collaboration[15, 16] (RSC), a group of experimentalists, theorists, and accelerator physicists, was formed in 1991 with the objective of advancing the case for a polarized collider program at RHIC. The RSC proposal update containing sections on, (A) polarized collider operation of RHIC, (B) the PHENIX detector spin physics program, and (C) the STAR detector spin physics program, was approved by the PAC in October 1993. The cost estimated for instrumenting RHIC to provide polarized-beam capability is ≈$10M.

During the past year the RIKEN Spin Group (RSG) has undertaken an initiative to provide a large part of the polarized collider equipment. In addition, the RSG will fund a major upgrade of the PHENIX muon spectrometer, making feasible for the first time an extensive program of high-Q^2 measurements of single-muon and dimuon production. The present proposal, authored by an enlarged collaboration, *PHENIX/Spin*, addresses the physics program to be carried out with the *upgraded* PHENIX detector. The physics program described in the PHENIX subsection of the RSC proposal covered measurements feasible with the Conceptual Design Report (CDR)[25] version of PHENIX, including inclusive direct photon production and $W^\pm$ production via electron detection. As the case has already been made for this suite of measurements, the present proposal focuses only on new capabilities.

1.3 Outline of the Proposed PHENIX Muon Upgrade

The enhanced PHENIX muon spectrometer is shown in Figs. 1 and 2. The upgrade for spin physics consists primarily of the addition of a second muon end cap, significantly enhancing the dimuon acceptance for large pair masses. Also, in order to maximize acceptance and to extend kinematic coverage, muon identification is added to the two arms of the central magnet outside the shielding enclosure (Fig. 2).

As is shown in Sect. 2, very general considerations lead to the expectation that polarization effects will increase with increasing $\sqrt{\tau} \equiv M/\sqrt{s}$. The qualitative increase in acceptance is clear from Fig. 3 which compares the baseline PHENIX muon spectrometer with the enhanced versions. The acceptance was calculated at $\sqrt{s} = 50\ GeV$ but is approximately valid for higher energies as well (see Appendix A.).

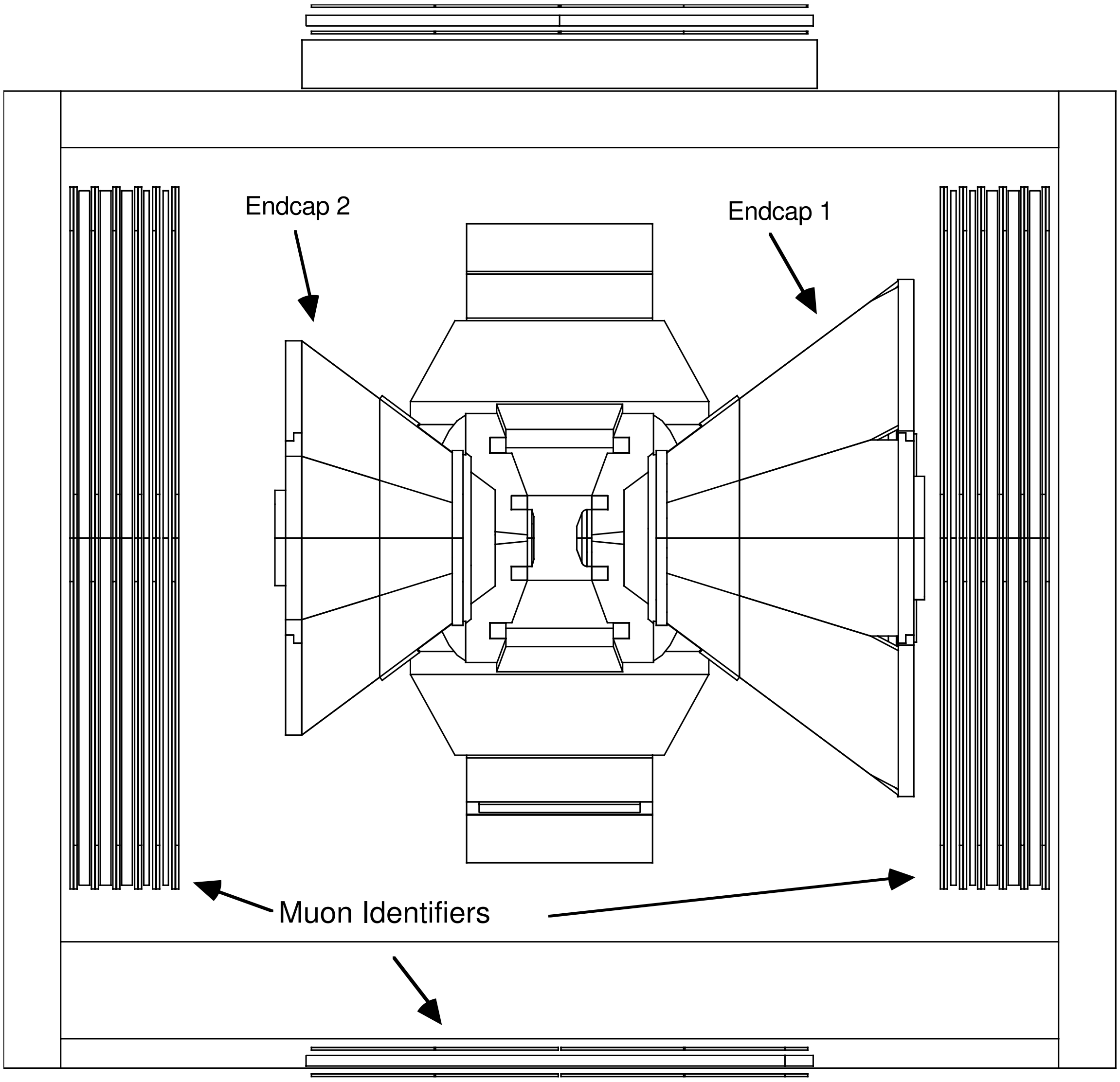

Figure 1: Plan view showing both muon end caps of the proposed upgraded PHENIX spectrometer. The first end cap (large triangle on the right) is the original muon arm of the PHENIX CDR[25]. The second end cap is shown on the left as a smaller triangle subtending the same angular range, $10° - 35°$. The muon identifiers of the two end caps are the vertical blocks of lines at the extreme right and extreme left, representing steel absorbers and muon chambers. Also shown at the top and bottom of the figure are muon chambers and absorbers proposed for the central magnet arms. The central muon identifiers are located outside the concrete shielding enclosure.

Figure 2: Elevation view down the beam axis showing the proposed muon identifier segments for the central magnet arms. The muon identifiers are located outside the concrete shielding enclosure. Also shown is the central magnet and selected detail of the dual detector arms.

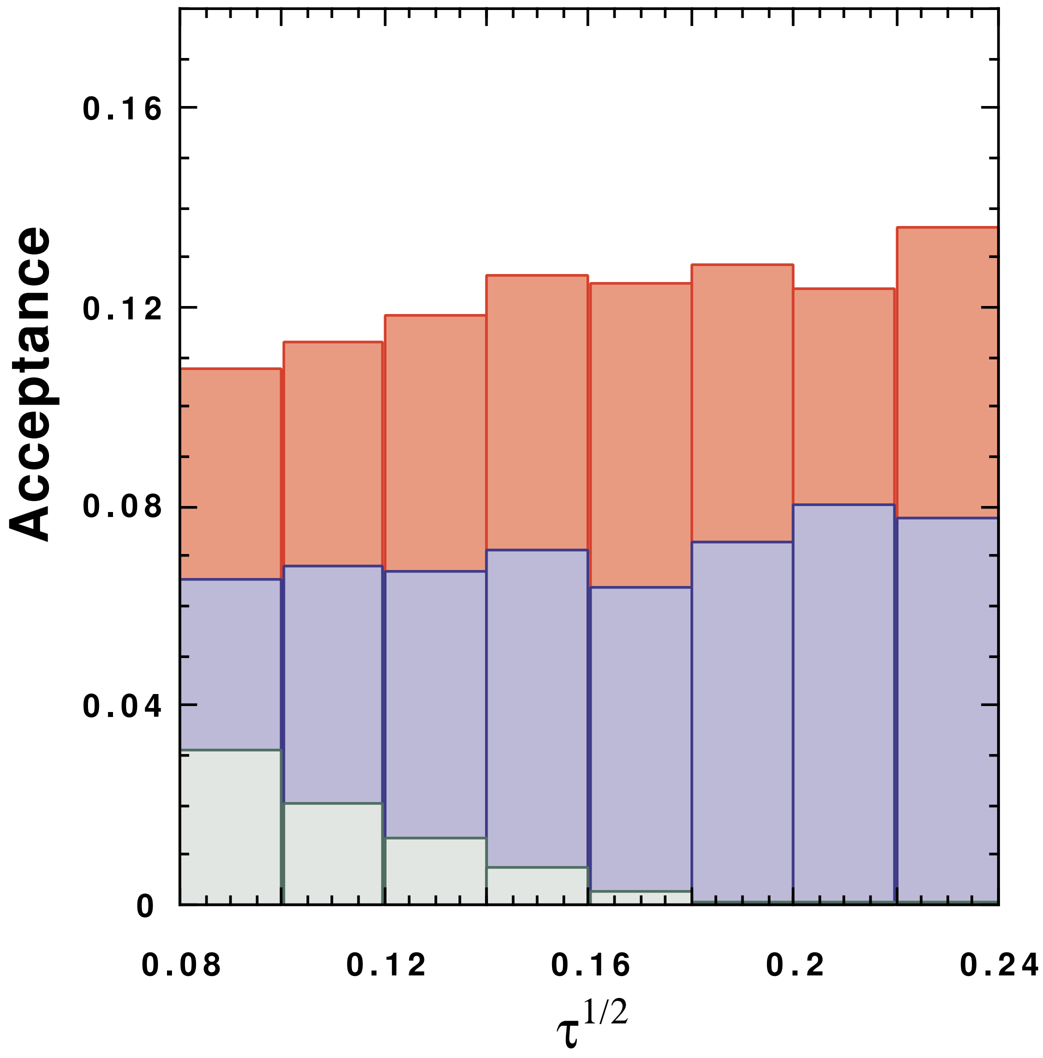

Figure 3: Dimuon mass acceptance for three versions of the PHENIX muon system; dotted, PHENIX baseline (1 end cap); hatched, 2 end caps; solid, 2 end caps plus muon identification in the central detector. The calculations were performed at $\sqrt{s} = 50\ GeV$ but are approximately valid at higher energies as well due to $\sqrt{\tau}$ scaling of the acceptance.

2 Spin Physics with the Enhanced PHENIX Muon Spectrometer

2.1 Antiquark Helicity Distribution Via the Polarized Drell-Yan Process

The Drell-Yan (DY) process[17], $q(x_1) + \bar{q}(x_2) \to \gamma^* \to \mu^+\mu^-$ (or e^+e^-, $\tau^+\tau^-$), has been studied for over twenty years, largely by measuring muon pairs in fixed target experiments at Fermilab and CERN[18]. With the advent of QCD descriptions, including next-to-leading-order corrections, it can be characterized as well understood theoretically[18]. Phenomenological evaluations of parton structure functions now routinely use DY as well as DIS data. The parton-model expression for the DY cross section,

$$M^3 \frac{d^2\sigma}{dM\,dx_F} = \frac{8\pi\alpha^2}{9}\frac{x_1 x_2}{x_1+x_2} \times \sum_a e_a^2[q_a(x_1)\bar{q}_a(x_2) + \bar{q}_a(x_1)q_a(x_2)], \tag{1}$$

is often multiplied by a factor, $K \approx 2$, which accounts for next-to-leading order QCD effects.

We first consider the measurement of A_{LL} in the DY process, since its close relation to A_{LL} of DIS experiments allows a reasonably quantitative analysis. The expression for the longitudinal spin asymmetry in the DY process has the simple form[8, 14],

$$A_{LL}^{DY}(x_1, x_2) = \frac{\sum_a e_a^2 \Delta q_a(x_1)\Delta\bar{q}_a(x_2) + (2 \leftrightarrow 1)}{\sum_a e_a^2 q_a(x_1)\bar{q}_a(x_2) + (2 \leftrightarrow 1)}, \tag{2}$$

with $\Delta q_a \equiv q_a^+ - q_a^-$. The superscripts refer to parton spin projections parallel (+) or antiparallel (-) to the parent hadron's spin projection. For $x_F \geq 0.2$ the denominator of Eq. 2 is dominated by the term, $q_u(x_1)\bar{q}_u(x_2)$, allowing a substantial simplification,

$$A_{LL}^{DY}(x_1, x_2) \approx \frac{\Delta u(x_1)}{u(x_1)} \times \frac{\Delta\bar{u}(x_2)}{\bar{u}(x_2)} + \frac{1}{4}\frac{\Delta d(x_1)}{u(x_1)} \times \frac{\Delta\bar{d}(x_2)}{\bar{u}(x_2)}, \tag{3}$$

where the notation $q_u(x) \equiv u(x)$ has been introduced. Neglecting small sea-quark effects, one can use approximate expressions for the structure functions of DIS,[3]

[3]The approximate forms for the structure functions of DIS used here are, $F_1(x) = 1/2\sum_a e_a^2 q_a(x)$ and $g_1(x) = 1/2\sum_a e_a^2 \Delta q_a(x)$.

$$F_1^p(x) \approx 2/9 \times u(x),$$
$$\Delta u(x) = 18/15(4g_1^p(x) - g_1^n(x)), \quad (4)$$
$$\Delta d(x) = 18/15(-g_1^p(x) + 4g_1^n(x)),$$

to achieve an important further simplification. The measured values of $g_1^{p,n}$ in DIS are shown in Figs 4 and 5. For $x \geq 0.2$ one sees that $g_1^n \approx 0$, and with the above relations Eq. 3 becomes,

$$\begin{aligned} A_{LL}^{DY}(x_1, x_2) &\approx A_{LL}^{pDIS}(x_1) \times [\frac{16}{15}\frac{\Delta\bar{u}}{\bar{u}}(x_2) - \frac{1}{15}\frac{\Delta\bar{d}}{\bar{u}}(x_2)], \\ &\approx A_{LL}^{pDIS}(x_1) \times \frac{\Delta\bar{u}}{\bar{u}}(x_2). \end{aligned} \quad (5)$$

The second step follows if $\Delta\bar{u} = \Delta\bar{d}$. Equation 5 has the familiar form of an experimentally measured asymmetry being determined by the product of a beam polarization and the asymmetry of a physical process. Thus for the DY process with $x_F \geq 0.2$, a longitudinally polarized proton can be thought of as a beam of *polarized* u quarks with $P_u(x) \approx A_{LL}^{pDIS}(x)$. It is apparent from the large measured values of $A_{LL}^{pDIS}(x_1 \geq 0.2)$ that longitudinal spin asymmetry in the DY process will be a sensitive measure of the polarization of the $\bar{u}$ quark distribution of the proton.

Equation 5 permits estimates to be made for actual experimental conditions, given some assumptions about the antiquark polarization. Until recently little guidance could be found on the subject of antiquark polarization beyond the strong indication that the strange quark sea makes a significant integral contribution to the proton's spin[3, 4, 5]. Bourrely and Soffer[19] adopt an approach to quark and antiquark polarization inspired by a possible connection between light-flavor asymmetries and spin asymmetries. Two recent experiments[20, 21] strongly suggest $\bar{u} \neq \bar{d}$ in the proton. Bourrely and Soffer propose,

$$\Delta\bar{u} = \bar{u}(x) - \bar{d}(x), \quad (6)$$

where the relation is fixed at $x = 0.18$ by a recent measurement of the $\bar{d}/\bar{u}$ asymmetry of the proton using the DY process[21].

Equations 1 (including a K-factor of 2) and 5 can be used with the model of Ref.[19] to make sensitivity estimates for realistic running conditions. Monte Carlo DY events are thrown in to the full acceptance of the enhanced PHENIX muon spectrometer, with 100% detection efficiency assumed for single muons above 2 GeV in the end caps, and above 1.3 GeV in the central arms. The luminosity of RHIC is assumed[16] to be $L = 2 \times 10^{32} \times (\sqrt{s}/500)\ cm^{-2}sec^{-1}$. Results at $\sqrt{s} = 50\ GeV$ for an integrated luminosity $\mathcal{L} = 2\times10^{38}cm^{-2}$ are shown in Fig. 6; beam polarizations were taken to be 0.7[16]. A total of 10.8 K muon pairs, $M \geq 4\ GeV$, are detected (Table 1). The errors on A_{LL} would be twice as large if measured at $\sqrt{s} = 200\ GeV$ with an integrated luminosity $\mathcal{L} = 8 \times 10^{38}cm^{-2}$ (see Appendix B). With

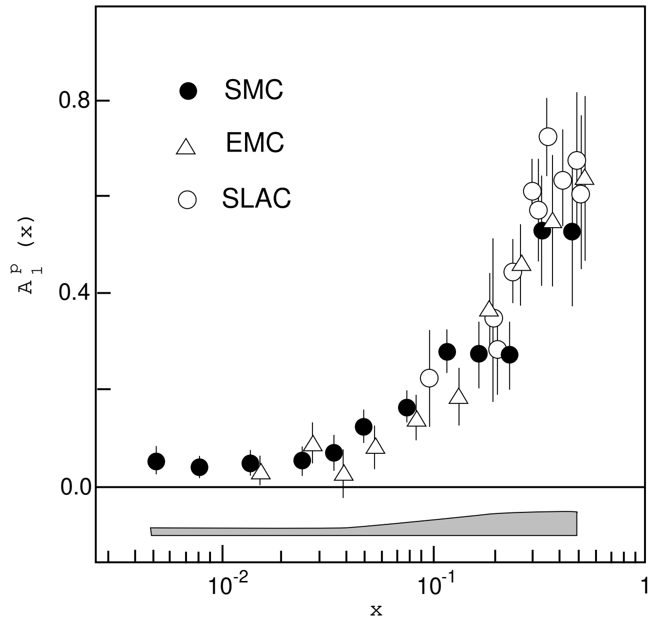

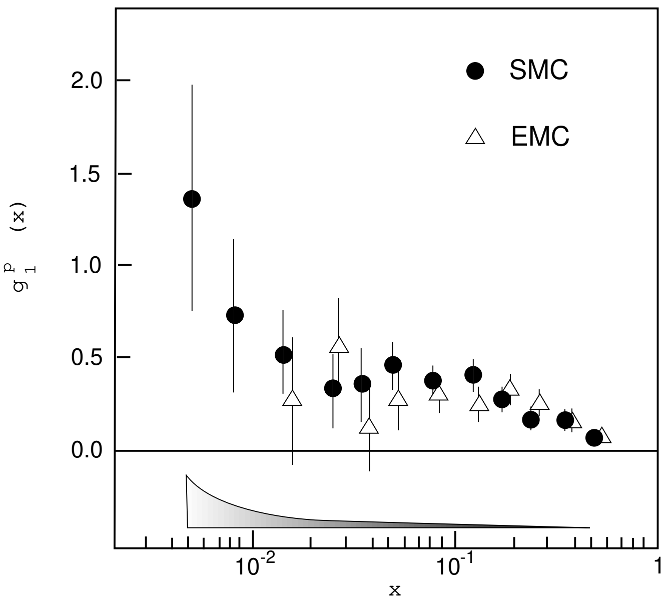

Figure 4: Longitudinal asymmetry and $g_1(x)$ structure function for deep-inelastic lepton scattering from the proton from CERN[1, 4] and SLAC[2]

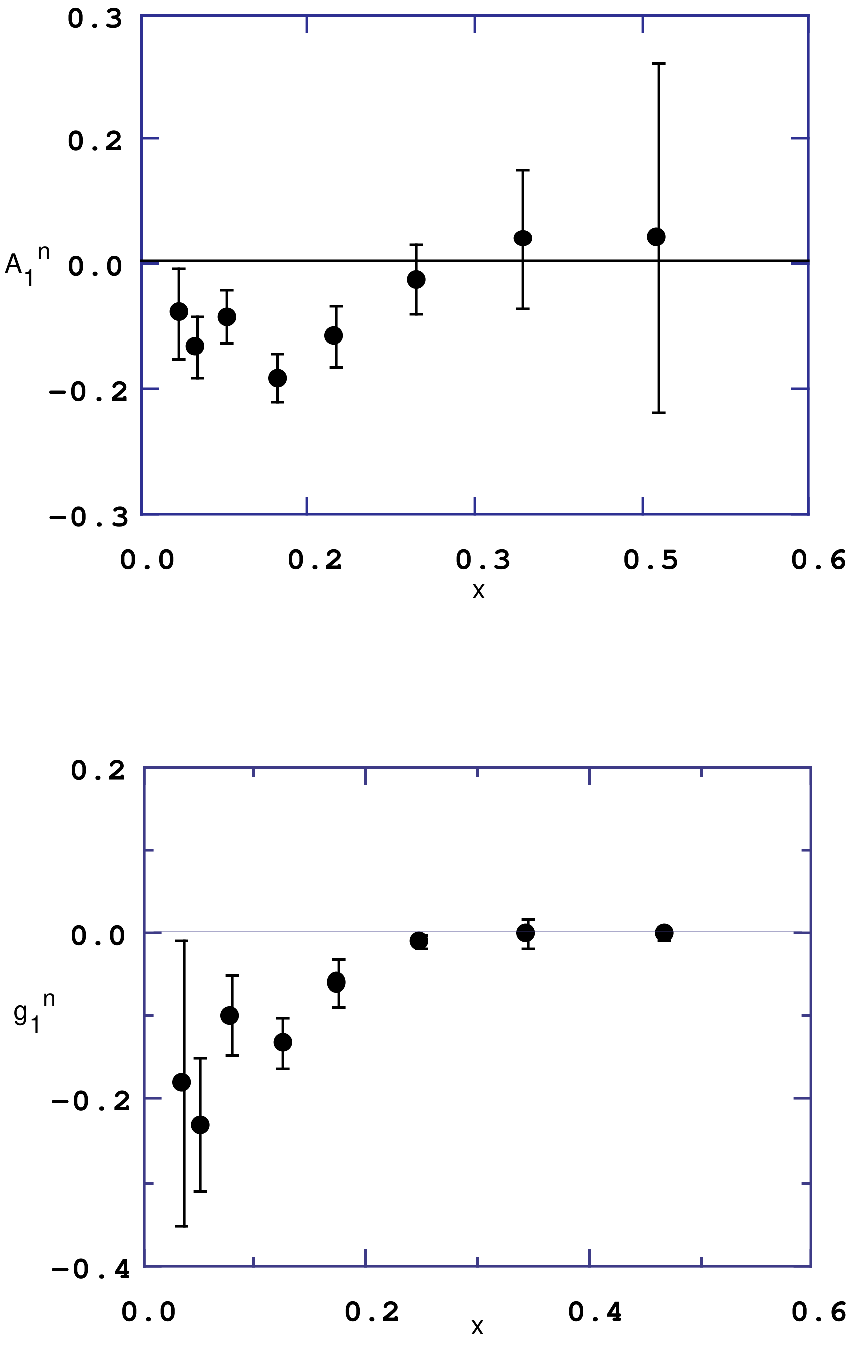

Figure 5: Longitudinal asymmetry and $g_1(x)$ structure function for deep-inelastic lepton scattering from the neutron (^3He) from SLAC[6]

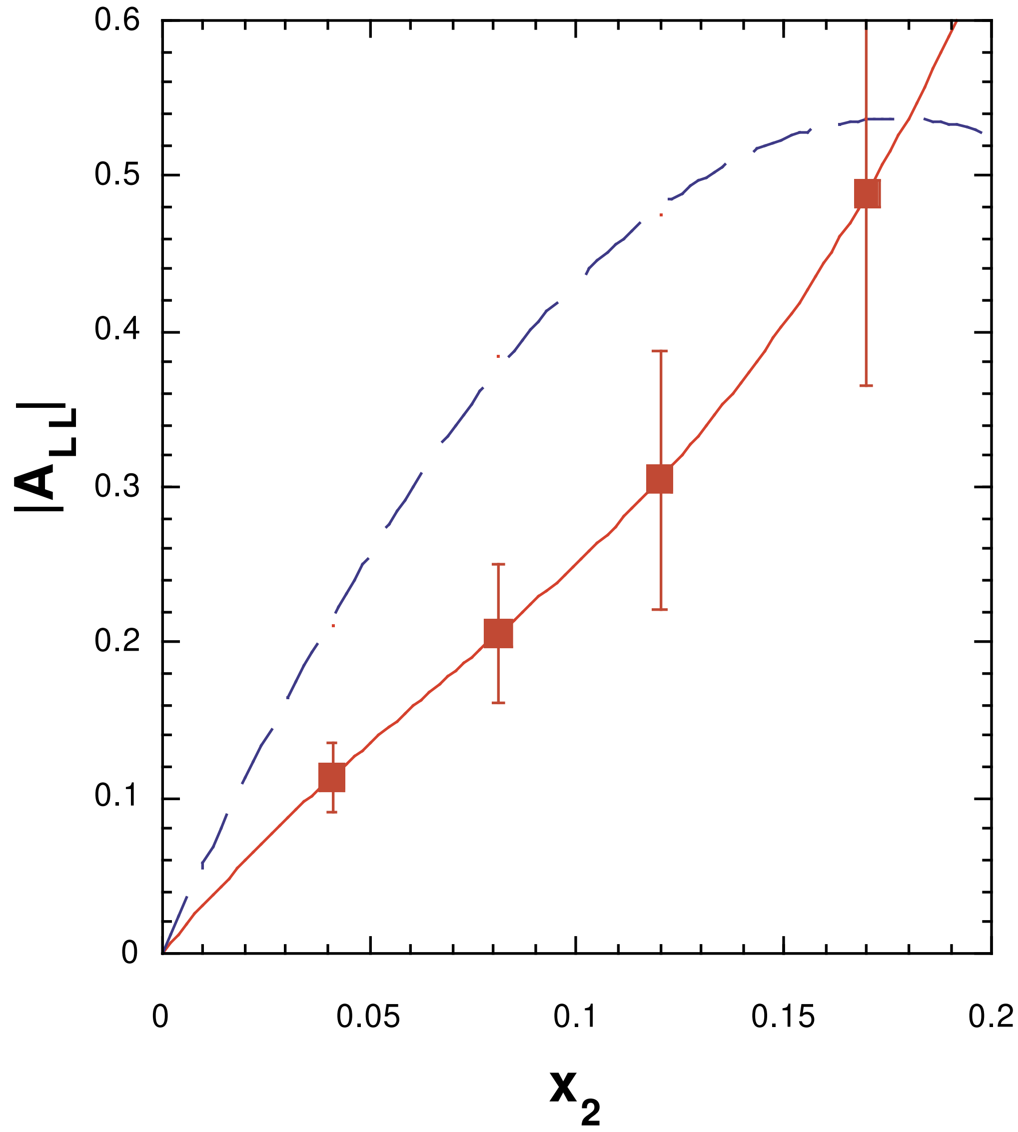

Figure 6: $|A_{LL}^{DY}|$ using Eq. 5 and the model of Bourrely and Soffer[19]. Two extrapolations consistent with the experimental results from CERN NA51[21] yield the two curves. Error bars (shown on the lower curve) are based on an integrated luminosity of $\mathcal{L} = 2 \times 10^{38} cm^{-2}$ at $\sqrt{s} = 50\ GeV$, yielding 10.8K muon pairs; beam polarizations are taken to be 0.7.

Mass Range (GeV)	4-6	6-8	8-10	$M \geq 10$
Number of dimuons	7930	1988	586	285

Table 1: Number of Drell-Yan dimuons detected by the upgraded PHENIX muon spectrometer at $\sqrt{s} = 50\ GeV$ with an integrated luminosity $\mathcal{L} = 2 \times 10^{38} cm^{-2}$.

the proposed PHENIX muon upgrade a sensitive measurement of the antiquark helicity distribution of the proton is clearly feasible.

Based on extensive experience with dimuon production in fixed-target experiments, the most serious source of background competing with the DY process is semileptonic charm decay. Drell-Yan production experiments at Fermilab[23, 24] ($\sqrt{s} = 38.7\ GeV$) provide strong evidence that the charm contribution is negligible for $M \geq 4\ GeV$. However extensive simulations performed for the PHENIX CDR[25] indicate competition from charm decay for $M \leq 5\ GeV$ at $\sqrt{s} = 200\ GeV$ where the production cross section is considerably larger.[4] Thus relatively low energies for DY physics are also indicated from the standpoint of background minimization.

2.2 Transversity Measurements in the Polarized Drell-Yan Process

The transversity structure function has recently received a great deal of attention[14, 15] as a potential source of qualitatively new insight into the spin structure of the nucleon; it is not measurable in DIS experiments. The transversity is defined in a fashion similar to Δq_a, specifically $\Delta q_a^T \equiv q_a^+ - q_a^-$ but with $\pm$ denoting the spin projection perpendicular to the momentum of the nucleon. It is measured in the DY process with transversely polarized beams. Specifically,

$$A_{TT}^{DY}(x_1, x_2) = \frac{sin^2\theta cos2\phi}{1 + cos^2\theta} \frac{\sum_a e_a^2 \Delta q_a^T(x_1) \Delta \bar{q}_a^T(x_2) + (2 \leftrightarrow 1)}{\sum_a e_a^2 q_a(x_1) \bar{q}_a(x_2) + (2 \leftrightarrow 1)}, \tag{7}$$

where θ is the polar angle of either lepton in the rest frame of the virtual photon, and ϕ is the angle between the direction of polarization and the normal to the plane of the dilepton decay.

Unlike $\Delta q_a(x)$, very little is known about $\Delta q_a^T(x)$. Estimates using the MIT bag model[14] indicate that $\Delta q_a^T(x) \geq \Delta q_a(x)$ in the large-x region where valence quark polarization predominates. No estimates are available for the antiquark transversity, $\Delta \bar{q}_a^T(x)$. We assume that optimization of the experimental conditions for $A_{TT}(x)$ is similar to that presented previously for A_{LL}. The major differences are in the angular dependencies of Eq. 7. For an axially symmetric detector the ϕ integration leads to a reduction of statistical precision of $1/\sqrt{2}$. Furthermore the θ dependence of the muon system is not all concentrated at 90°, as can been seen in Fig. 7, leading to a further small reduction in statistical precision. Thus, given equal magnitudes of helicity and transversity polarization effect, obtaining statistical significance for A_{TT} will be more difficult.

2.3 $W^{\pm}$ Production

Production of $W^{\pm}$ and Z^0 bosons at $\sqrt{s} = 500\ GeV$ at RHIC offers an important opportunity in polarized quark structure function physics, complementary to continuum DY production.

[4] The increase may be $\sim 6 - 10$ depending on the extrapolation used[26].

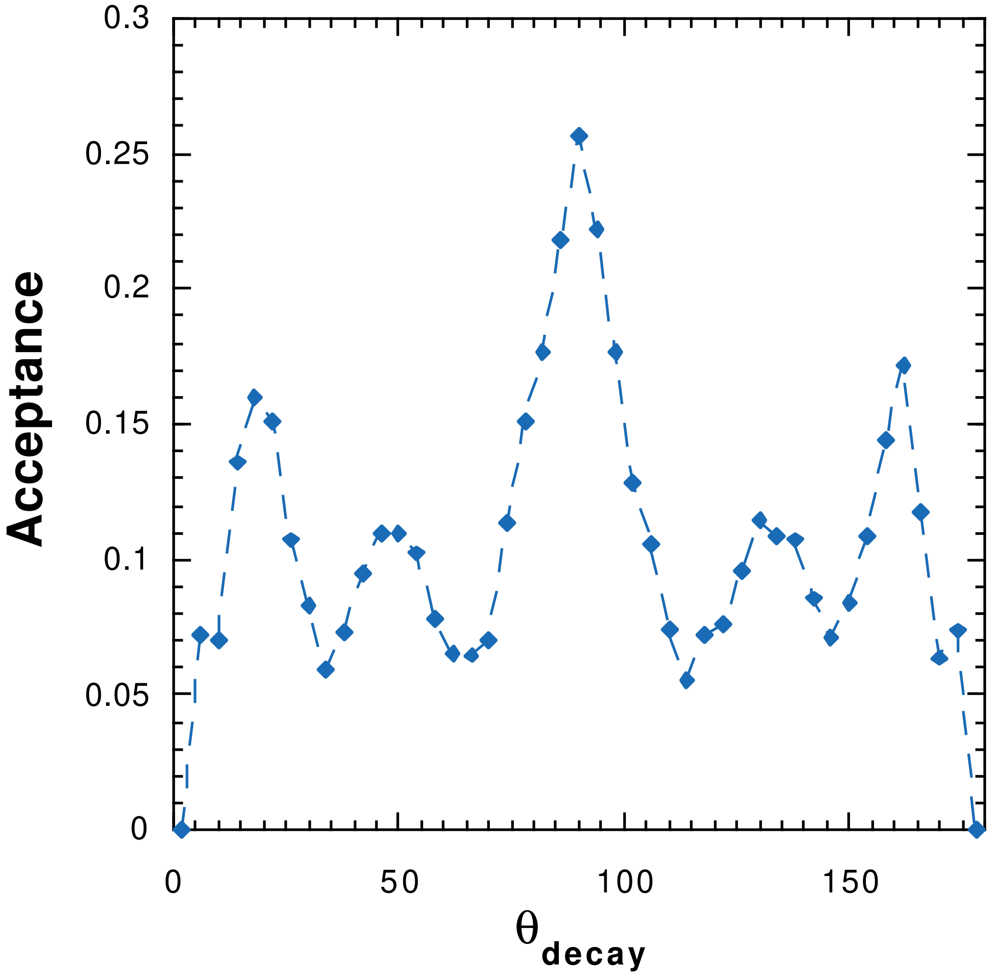

Figure 7: Decay angle acceptance of the upgraded muon spectrometer for Drell-Yan pairs with $\sqrt{\tau} \geq 0.8$.

As was emphasized in the RSC proposal[15], polarized-beam experiments present an opportunity for new physics discovery in the domain where the weak interaction predominates.

The cross section for W^+ production is given by,

$$d\sigma/dy = \sqrt{2}\pi G_F x_1 x_2 \times \frac{1}{3}[u(x_1)\bar{d}(x_2) + \bar{d}(x_1)u(x_2)], \tag{8}$$

where G_F is the Fermi coupling constant. The structure functions are evaluated at the mass scale of the vector bosons. Because $W^\pm$ production occurs via a purely left-handed current (in the Standard Electroweak Model) the helicity asymmetries are more complex than for the DY process. Bourrely and Soffer[19] define three parity violating asymmetries and one parity conserving asymmetry. They further show, with the reasonable approximation, $\Delta u \Delta \bar{d} \ll u\bar{d}$, that the parity violating single and double spin asymmetries contain the same information. For W^+ production the parity violating single-spin (measurable with a single polarized beam) and parity-conserving double spin asymmetries are given respectively by,

$$A_L^{pv}(x_1, x_2) = \frac{-u(x_1)\Delta\bar{d}(x_2) + \bar{d}(x_1)\Delta u(x_2)}{u(x_1)\bar{d}(x_2) + \bar{d}(x_1)u(x_2)}, \tag{9}$$

and,

$$A_{LL}^{pc}(x_1, x_2) = -\frac{\Delta u(x_1)\Delta\bar{d}(x_2) + \Delta\bar{d}(x_1)\Delta u(x_2)}{u(x_1)\bar{d}(x_2) + \bar{d}(x_1)u(x_2)}. \tag{10}$$

Using the model for antiquark polarization described in Sect. 2.1 A_L has been calculated[19] for $\vec{p}\vec{p}$ collisions at $\sqrt{s} = 500\ GeV$; the calculations are shown in Fig 8.

Polarization effects in $W^\pm$ production are measured by detection of single high-p_t muons, an inclusive process that integrates over a range of x_1 and x_2. The PHENIX end caps have very short ($\sim 0.5\ m$) decay distances which effectively discriminate against muons from pion and kaon decay and are hence ideal for high-momentum single muon detection. The principal background to the $W^\pm$ signal is from muon decay of heavy quarks. Based on experience at $p\bar{p}$ colliders[28, 29], the most effective method of discriminating against heavy-quark decays is to use only the highest p_t part of the spectrum.[5] Figure 9, an ISAJET calculation for the PHENIX end caps at $\sqrt{s} = 500\ GeV$, shows that the region $p_t \geq 30\ GeV$ is dominated by $W^\pm$ decays. This threshold results in a combined acceptance in the two end caps of 10%, yielding production of $\approx$ 24K (9K) W^+ (W^-) events with $\mathcal{L} = 2 \times 10^{39} cm^{-2}$.

The high p_t cut also limits the acceptance to the large x_F kinematic range, $\langle x_F \rangle = 0.375$, where simplifications in the spin asymmetries similar to those discussed in Sect. 2.1 apply. Under these conditions Eq. 9 yields,[6]

$$A_L^{pvW^+} \approx -\frac{\Delta\bar{d}}{\bar{d}}(x_2), \text{ and } \quad A_L^{pvW^-} \approx -\frac{\Delta\bar{u}}{\bar{u}}(x_2) \tag{11}$$

[5]We do not speculate on the efficacy of isolation cuts since PHENIX does not resemble any of the operational collider detectors. Extensive simulations are required to deal with this issue in a realistic way.

[6]The $+y$ (x_F) solutions (Fig. 8) correspond to valence quark ratios at $x \approx 0.35$ which are better measured in DIS experiments.

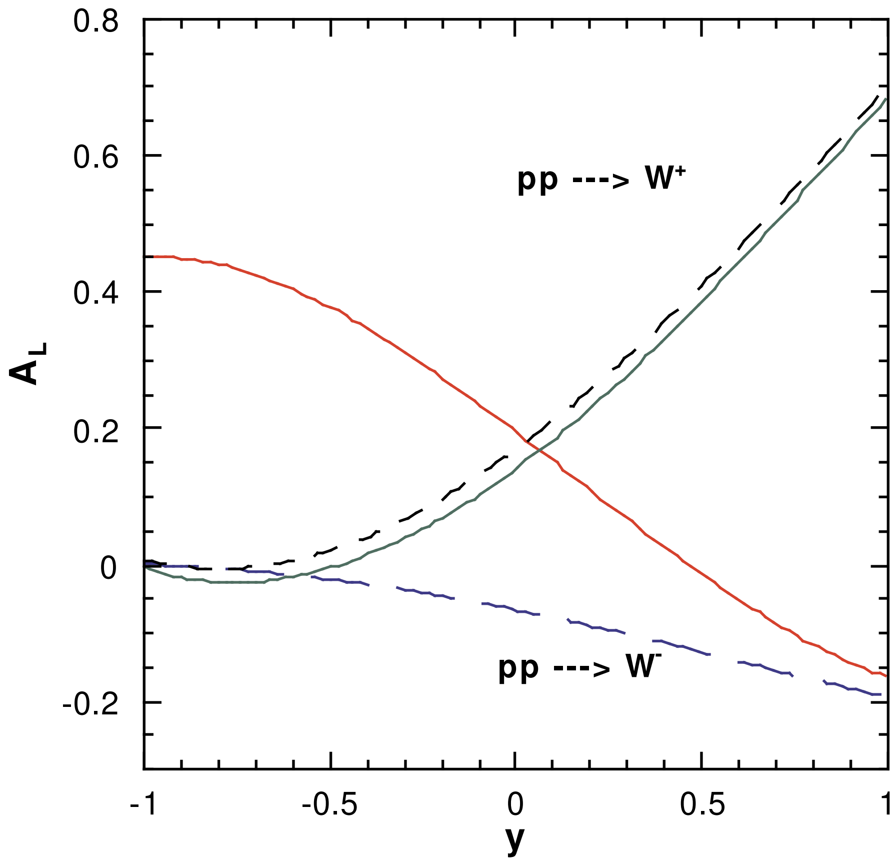

Figure 8: Parity violating asymmetries for $W^{\pm}$ production at $\sqrt{s} = 500\ GeV$. The solid lines use the antiquark polarization as described in Ref. [19]; the dashed lines correspond to $\Delta\bar{u} = \Delta\bar{d} = 0$.

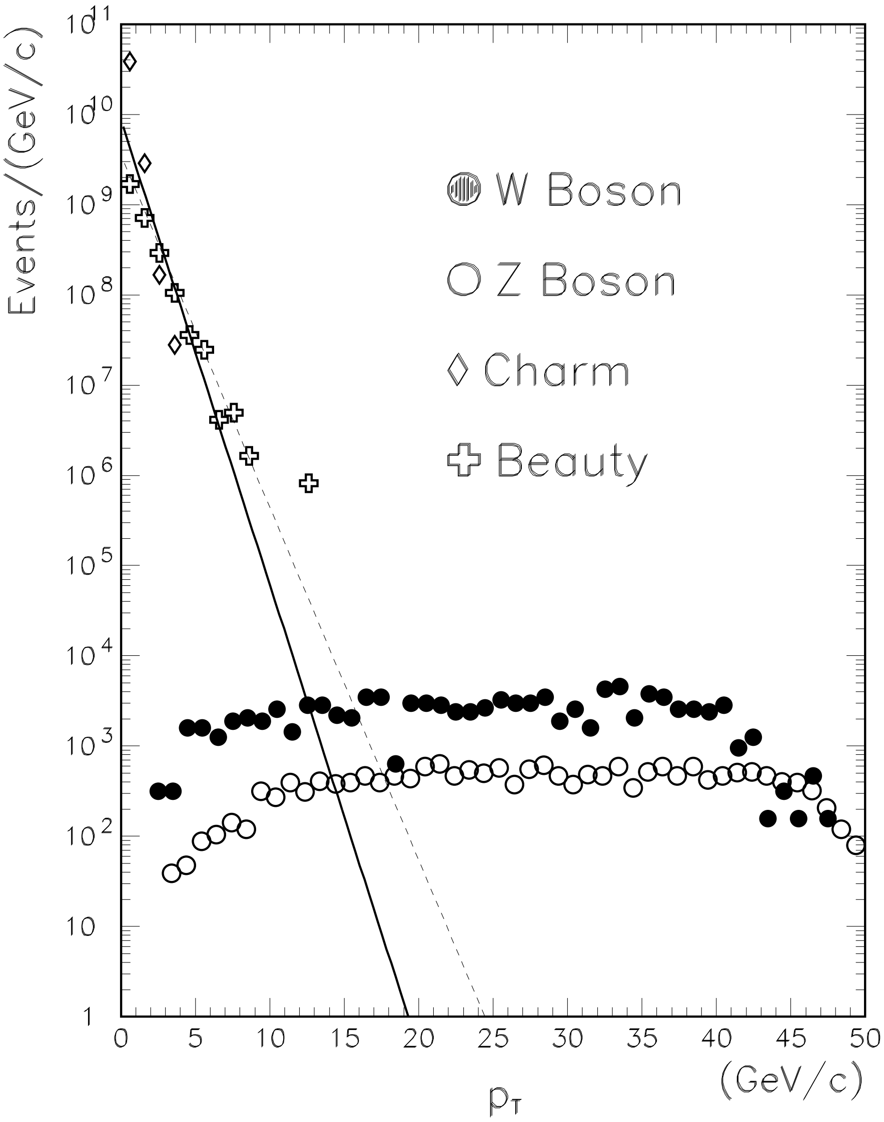

Figure 9: Production of single muons from charm, beauty, and vector boson decay into the PHENIX end caps at $\sqrt{s} = 500\ GeV$ using ISAJET. The lines show two possible extrapolations of the beauty decays to higher transverse momenta where the calculation has insufficient statistical precision.

while Eq. 10 reduces to,

$$A_{LL}^{pcW+} \approx \frac{\Delta u}{u}(x_1) \times \frac{\Delta \bar{d}}{\bar{d}}(x_2) = A_{LL}^{pDIS}(x_1) \times \frac{\Delta \bar{d}}{\bar{d}}(x_2), \tag{12}$$
$$A_{LL}^{pcW-} \approx \frac{\Delta d}{d}(x_1) \times \frac{\Delta \bar{u}}{\bar{u}}(x_2).$$

The second step for W^+ production shows the similarity to the DY process, Eq. 5. Thus both the parity violating and parity conserving asymmetries provide a measure of the ratio of the polarized to unpolarized antiquark structure functions at $x_2 \approx 0.06$ (range roughly $0.04 \leq x_2 \leq 0.1$). Based on the number of W^- events estimated above, the errors on $\Delta\bar{u}/\bar{u}$ from the use of Eq. 11 would be comparable to those obtainable via the DY process in the same x_2 range.

2.4 Z^0 Production

The enhanced PHENIX dimuon system is ideal for detection of the decay branch $Z^0 \rightarrow \mu^+\mu^-$ over a large x_F range (Fig. 10) with an integrated acceptance of $\approx$ 18%. There are no processes likely to contribute any significant background. ISAJET calculations at $\sqrt{s} = 500\ GeV$ give $\sigma \times B_{\mu\mu} = 13.3\ pb$, yielding $\approx 5.0K$ events with $\mathcal{L} = 2 \times 10^{39} cm^{-2}$.

Bourrely and Soffer[27] emphasize the application of Z^0 production to the determination of the transversity structure function. The much larger values of x and Q^2 would make this process complementary to transversity or helicity measurements in DY production.

Electroweak interference effects are maximized at the mass of the Z^0, leading to the possibility of precise tests of QCD corrections to the elementary production mechanism. For example interference between photon and Z^0 exchange modifies the $1 + cos^2\theta$ angular distribution characteristic of the DY process. Near the Z^0 mass one has, $d\sigma/d\Omega \propto A + Bcos^2\theta + Ccos\theta$. The charge asymmetry term, $C\cos\theta$, has been measured in unpolarized $p\bar{p}$ collisions at the Tevatron Collider by CDF[30]. We are currently examining the implications of this term for polarized proton collisions.

2.5 Gluon Polarization Effects in Heavy Quark Production

Polarization of the gluon field has attracted considerable attention, in connection with the axial anomaly,[7] as a possible source of the "missing" spin of the proton. A variety of models have been published on the subject of gluon polarization[31, 32, 33, 34].

Quarkonium[35, 36, 37] production and open heavy-flavor production[37] have both been considered as possible means for the delineation of gluon polarization effects.[8] The advantages of heavy quark production are its large cross section and surprisingly large parton-level asymmetries. Quarkonium production has the further merit that its decay width to dimuons is large and easily detectable.

[7]See, for example, the discussion by Jaffe and Manohar[3].

[8]Heavy quark production is known to be dominated by gluon fusion in the RHIC energy range. Contributions from $q\bar{q}$ fusion compete with gluon fusion at very large x_F but are generally a small part of the total cross section. Production of the J/ψ via b-quark decay may be appreciable at $\sqrt{s} = 500\ GeV$.

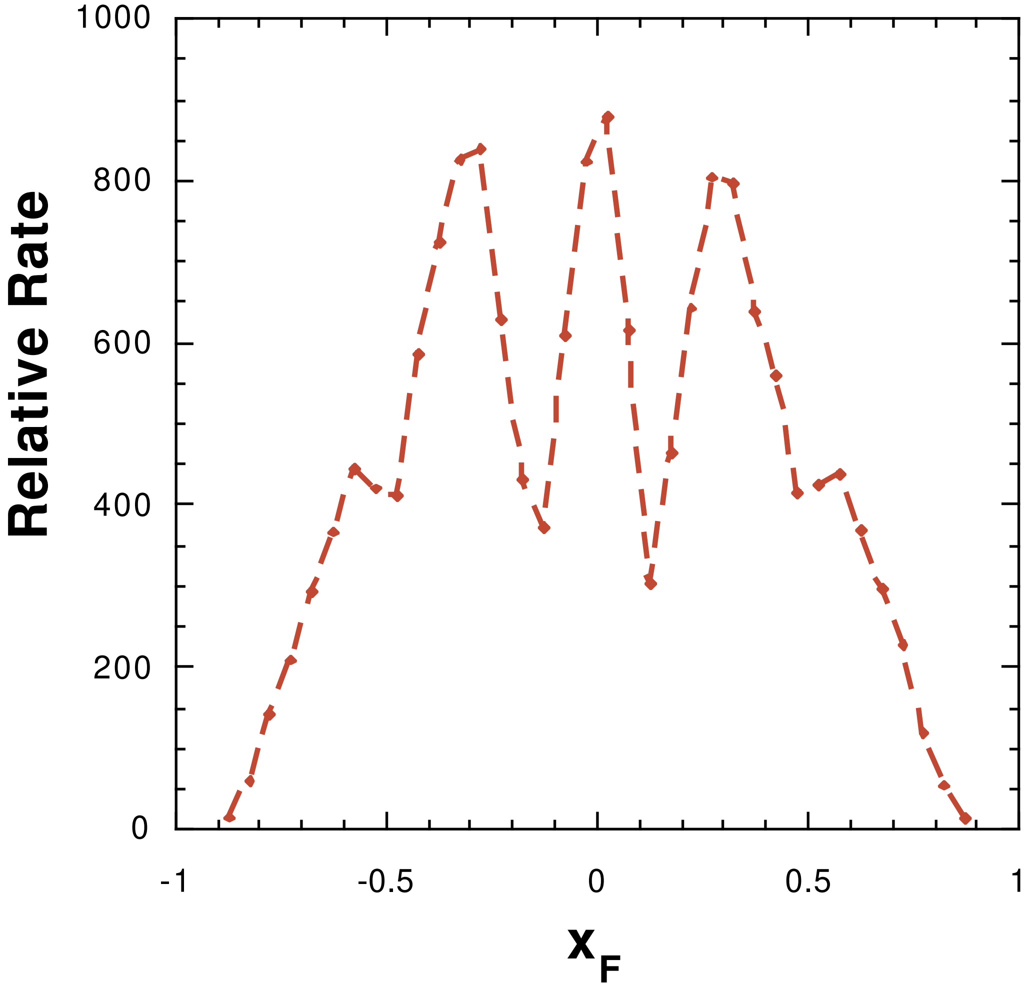

Figure 10: Acceptance versus x_F for $Z^0 \to \mu^+\mu-$ at $\sqrt{s} = 500\ GeV$.

$\sqrt{s}$	J/ψ	ψ'	$\Upsilon(1S)$
50	5.8×10^5	7.3×10^3	4.3×10^2
200	1.1×10^7	1.6×10^5	1.8×10^4
500	3.0×10^7	4.3×10^5	6.8×10^4

Table 2: Numbers of pairs accepted into the upgraded PHENIX spectrometer for an integrated luminosity of $2 \times 10^{39} \times (\sqrt{s}/500)$.

In general one can write,

$$A_{LL}(x_1, x_2) = \frac{\Delta G}{G}(x_1) \times \frac{\Delta G}{G}(x_2) \times \hat{a}_{LL}(\hat{s}, \hat{t}, \hat{u}), \tag{13}$$

where $\hat{a}(\hat{s}, \hat{t}, \hat{u})$ is the parton level asymmetry for the particular gluon fusion process.[9]

2.5.1 J/ψ , ψ' , and Υ production

Asymmetries for J/ψ and Υ production are usually discussed in terms of parton fusion models which rely on bound-state phenomenology[38] for identifying various possible production mechanisms. Two paths which are likely to contribute to J/ψ (Υ) production are,

$$g + g \to \chi_2 \to J/\psi(\Upsilon) + \gamma, \tag{14}$$

and

$$g + g \to J/\psi(\Upsilon) + g. \tag{15}$$

One expects the ψ' resonance to be produced primarily via the second path, since its mass lies above the χ region. The parton-level asymmetry for indirect production via the χ_2 state is maximally large and independent of kinematics, $\hat{a}_{LL}^{\chi_2} = -1$. Theoretical evidence[36, 38] and experimental data from hadron production of $J/\psi s$ [39] suggest that $\sim 30 - 50\%$ of the cross section is via this path at fixed-target energies. Unfortunately the asymmetry for the three-gluon mechanism has the opposite sign to the χ_2 production path, resulting in cancellation[36]. In the dominant kinematic region, $\hat{s} \sim M_{Q\bar{Q}}$, one finds[36] $\hat{a}_{LL}^{3g} \approx 0.2 - 0.3$. Nevertheless, using a model which includes both direct and indirect production of the J/ψ and Υ resonances, Doncheski and Robinett[36] predict sizable values, $A_{LL} \approx 0.2$, near $\sqrt{\tau} = 0.1$.

Production of the J/ψ , ψ' , and Υ resonances[10] produces substantial yield in the dimuon channel in the RHIC energy range as is evident in Table 2.

Lower limit errors (neglecting background subtraction and systematic errors) may be calculated as $\delta A_{LL} \approx 1/(P_b^2\sqrt{N})$, where $P_b \approx 0.7$ is the proton beam polarization.

[9]Next-to-leading order corrections to the equations used in this section have not been evaluated. There is, of course, the possibility that these corrections could substantially modify the polarization relations.

[10]Upsilon physics at low $\sqrt{s}$ is only feasible with a 2-end cap muon detector, as is evident from Fig. 3.

In order to get a qualitative picture of asymmetries in quarkonium production, Fig. 11 shows $|A_{LL}|$ for several published structure functions[31, 32, 33, 34]. Equation 13 has been used with $\hat{a}_{LL} = 0.3$, approximating the cancellation between the two production mechanisms as calculated by Doncheski and Robinett[36]. The polarized structure functions of Refs.[31, 32, 33] have the property $\Delta G(x) \propto xG(x)$ over much of the x range. Equation 13 then becomes,

$$A_{LL}(x_1, x_2) \rightarrow A_{LL}(\tau) \propto \tau \times \hat{a}_{LL}. \tag{16}$$

Thus there is no dependence on x_F, and polarization effects increase linearly with τ. The points in Fig. 11 are plotted on the curve of Ref.[32] with errors determined by the numbers of Table 2. Both J/ψ and Υ data would be most significant in constraining the current models at the lowest collision energy.

2.5.2 Inclusive Heavy Flavor Production

Open charm and beauty production will have significant cross sections in the RHIC operating range. PYTHIA calculations indicate $\sigma_{c\bar{c}} \approx 170\mu b$ and $\sigma_{b\bar{b}} \approx 2\mu b$ at $\sqrt{s} = 200\ GeV$. Additionally, the parton-level asymmetry is expected to be large for $\hat{s} \gg m_Q$[37]. This strongly suggests that the inclusive high-p_t single muon spectrum or $\mu - e$ coincidences could be used to measure an integral value of $\Delta G/G$ with high statistical precision. Figure 12 shows the number of inclusive single muons detected by the muon end caps for $\sqrt{s} = 200\ GeV$, $\mathcal{L} = 8 \times 10^{38} cm^{-2}$ compared to the pion decay background. Using the values of the asymmetry for charm and beauty decay averaged over the end cap acceptance for $p_t \geq 3\ GeV$ yields $\hat{a} \approx -0.4$. With $\sim 10^7$ counts this would yield a very significant measurement of $\Delta G/G$ at $x \sim 0.05$.

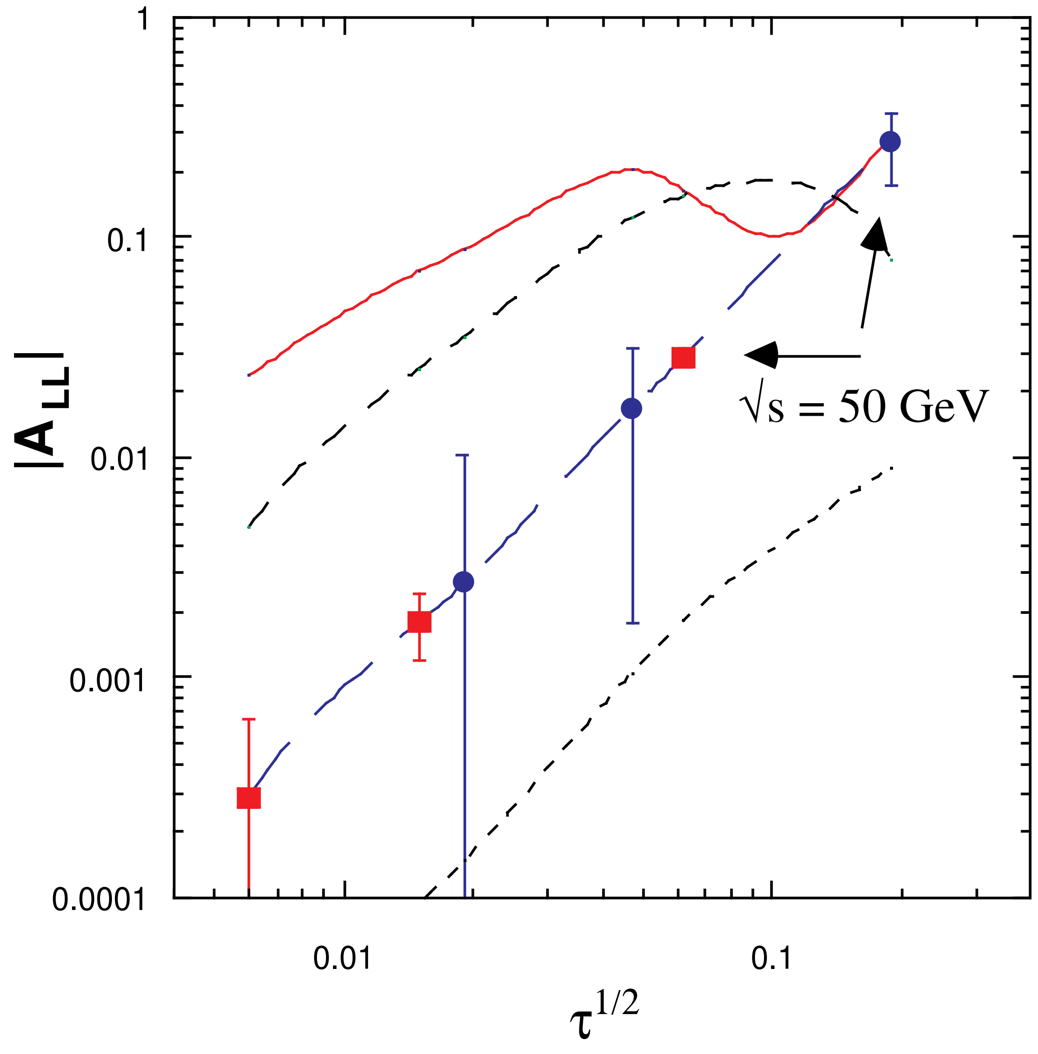

Figure 11: Asymmetries using the polarized structure functions of Ref.[34] (solid), Ref.[33] (medium dash), Ref.[32] (long dash), and Ref. [31] (short dash). A parton-level asymmetry, $|\hat{a}| = 0.3$ has been assumed. The points show error estimates for J/ψ (squares) and Υ (circles) production described in the text.

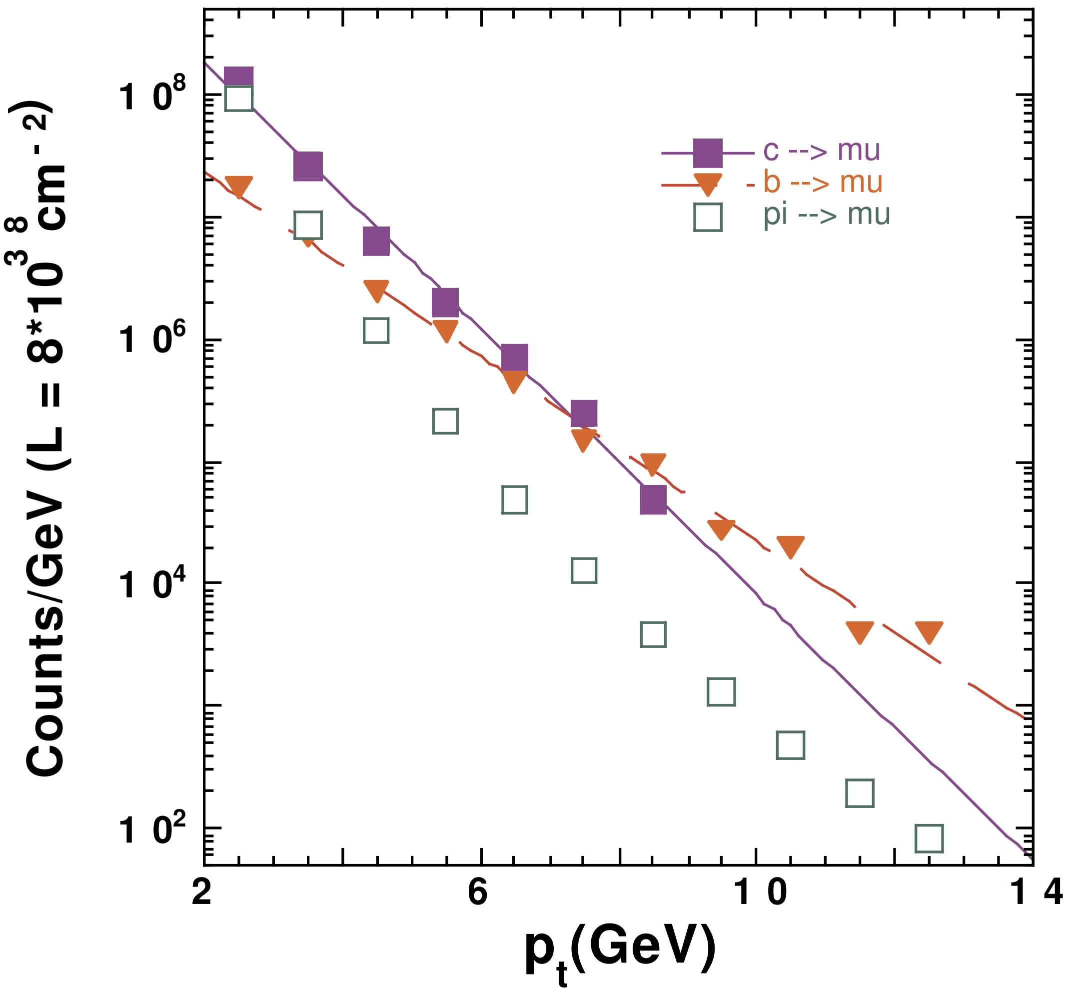

Figure 12: Production of single muons from charm, beauty, and pion decay into the PHENIX end caps at $\sqrt{s} = 200\ GeV$ versus p_t . Straight lines have been drawn through the charm and beauty decay distributions to aid in the clarity of the presentation.

3 The PHENIX Muon Spectrometer Upgrade

3.1 The Second Muon Arm

There are several options under study which would allow integration of the second arm into the PHENIX construction project. In order to have access to the detector systems of the first muon arm and of the central arms, the central magnet must be moved along the beam direction toward arm 2. With the shield wall removed, complete disassembly of the detector can then be accomplished by moving the central magnet and attached detector systems laterally away from the beam line. To preserve this access the second muon arm must be somewhat shorter than the first. A solution which appears promising is to shorten the second arm by 1.5 m as is depicted in Fig. 1. This requires arm 2 to be movable along the beam line. Because the magnetic lever arm is less there will be a degradation in the mass resolution if the angular range of the second arm is identical to the first. PISA simulations indicate an increase in the width of the Υ from $\sigma \approx 150$ MeV for arm 1 to $\sigma \approx 200$ for arm 2. Alternately the second arm could have a piston structure with more iron, resulting in a larger field and improved mass resolution. For example, an increase in the inner angle from 10° to $\approx 13^\circ$, would result in a field integral comparable to the first arm, with a consequent small loss of acceptance.. The most physics-effective way to strike this compromise (and others) is under active study.

3.2 Muons in the Arms of the Central Magnet

Detection of muons in the dual arms of the central magnet produces a significant increase in acceptance for high-$\sqrt{\tau}$ muon pairs, as is shown by Fig. 3. Most of this increase arises from the detection of one muon in a central arm and the other in an end cap. This combination also produces acceptance in the regions, $0.01 \leq x \leq 0.02$ and $0.04 \leq x \leq 0.09$, which are otherwise inaccessible as is evident in Fig. 13. This kinematic region is extremely important for the study of shadowing in pA and AA collisions. Shadowing is observed in nuclear quark distributions in DIS experiments for $x \leq 0.05$.

The large radius (5 m) to the beginning of the electromagnetic calorimeter is hardly ideal for suppressing pion and kaon decays. However we envision use of the central arms primarily for the detection of high-mass dimuons. Here the exceedingly steep falloff of the hadron p_t spectrum combined with the small probability of having two such events nearly back to back leaves the high-mass range of the spectrum free from backgrounds. Figure 14 compares the rate of DY events entering the central arms with backgrounds from pion decay in pp collisions at $\sqrt{s} = 50\ GeV$. Even though the acceptance for true DY events in the central arms only is quite small, the background from pion decays is negligible for $M \geq 4\ GeV$. The background rate from kaon decay relative to pion decay is estimated to be lower by a factor of $\approx$4.

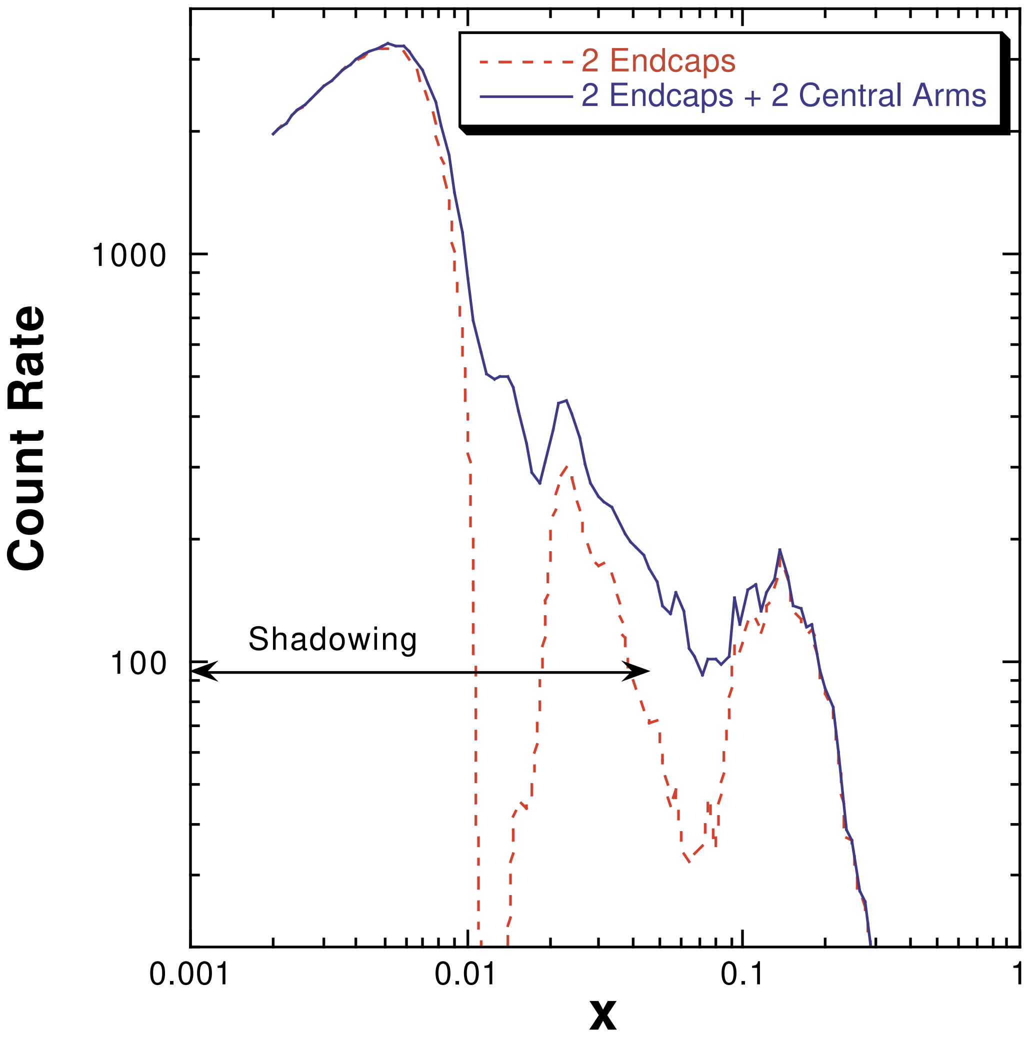

Figure 13: Acceptance of the upgraded PHENIX muon spectrometer for Drell-Yan pairs, $M \geq 4\ GeV$ at $\sqrt{s} = 200\ GeV$, versus x with and without muon detection in the arms of the central magnet. The arrow shows the expected region of nuclear shadowing in pA and AA collisions.

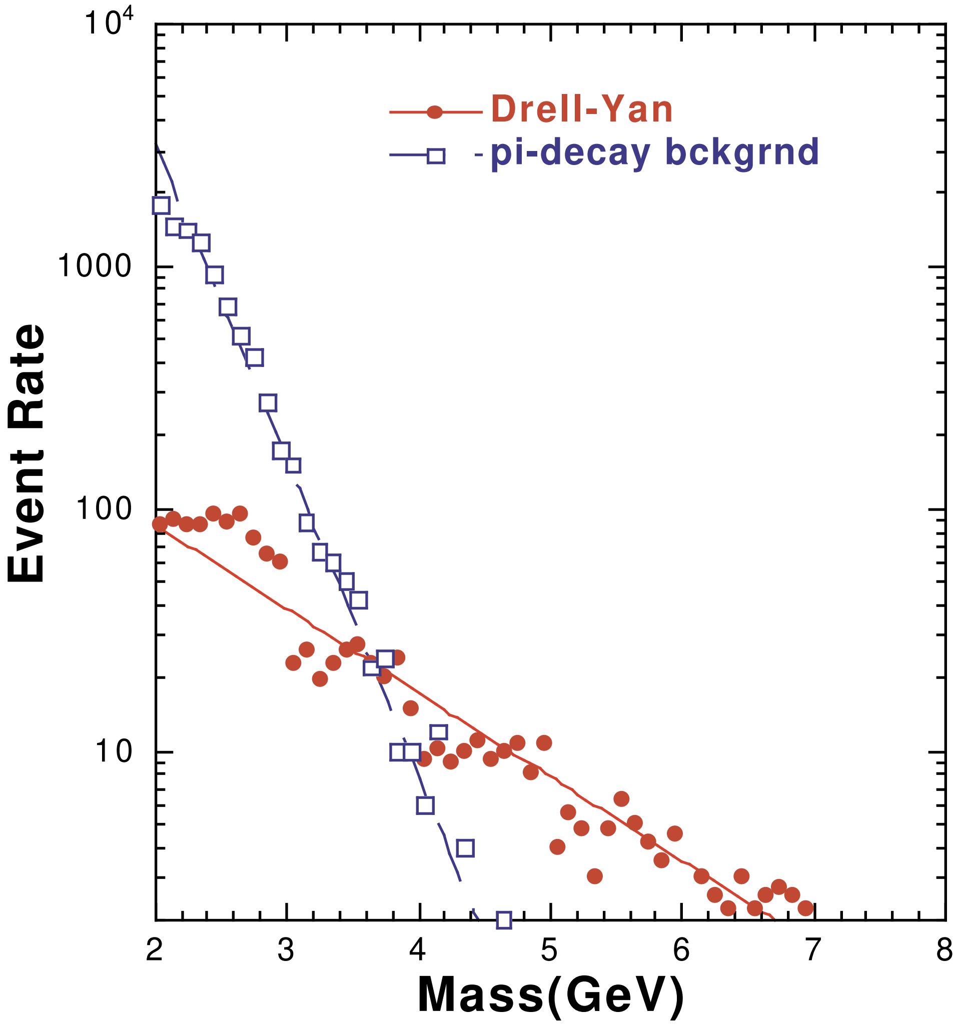

Figure 14: Simulation of Drell-Yan events in the central magnet arms compared to background from pion decays at $\sqrt{s} = 50\ GeV$. The simulations were performed with PISA[41], using pion production cross sections from Alper, *et al.* [42]. Perfect muon identification was assumed.

3.3 Detection of High-$\sqrt{\tau}$ Muon Pairs

The PHENIX CDR[25] and updates establish in great detail the feasibility of detecting dimuons from the DY process ($M \geq 4\ GeV$) and quarkonium production into the first muon end cap for rapidities $y \geq 1$ at $\sqrt{s} = 200\ GeV$. The mirror kinematic coverage of the second arm should be very similar. There may be some differences in the hadron absorption characteristics either due to a desire to have a lower muon threshold or to a physical difference in the configuration of the second arm.

The requirements on triggering, muon identification, and pattern recognition are considerably less stringent for *pp* physics than for the quark-gluon plasma (QGP) search program for which the first end cap was optimized. Because of the large effort which has gone into the design of the first end cap it is worth comparing the scale of the signal-to-background for the QGP and *pp* physics programs for the DY process. The comparison is made at equivalent luminosities, $A^2 \times L$, for $AuAu$ and $\vec{p}\vec{p}$ collisions. Backgrounds are taken to be dominated by random coincidences of either pion punch-through or muons from pion and kaon decay which emulate high-mass DY muon pairs. Compared to the *pp* background, the rate of soft hadron production from central $AuAu$ collisions is, $F \geq A_{Au}^{4/3}$, where "$\geq$" indicates that higher p_t production may well go as a higher power of A[40]. The background rate from random coincidences of such events is $B \sim F^2 \geq A_{Au}^{8/3}$. Again with reference to *pp* collisions, the rate of production of DY pairs in central heavy-ion collisions is $R_{DY} \sim A_{Au}^2$. Thus the overall signal-to-noise factor, R_{DY}/B, is $\geq A_{Au}^{2/3}$ (34) times better for the $\vec{p}\vec{p}$ program at equivalent luminosities.

The principal operational differences between dimuon detection as described in the Conceptual Design Report[25] and what is proposed here are connected with detection of rather low-energy muons near central rapidity. Here the opening angle between the muons is large enough that they are accepted into different arms (hence the increase in acceptance). Also, one or more muons may be detected in the arms of the central magnet. Optimization of the configuration of the second arm requires further simulation for polarized proton physics as well as investigation of its performance for the QGP program. As an example, it may be desirable to have less total hadronic absorption in the second arm in order to lower the minimum mass threshold for central J/ψ and ψ' events. Figure 15 shows that operation of the second arm without the "nose cone" hadron absorber of the first arm permits recording of J/ψ events well above the pion decay continuum. Clearly J/ψ production in low multiplicity $\vec{p}\vec{p}$ collisions is feasible even without maximal suppression of hadron decays.

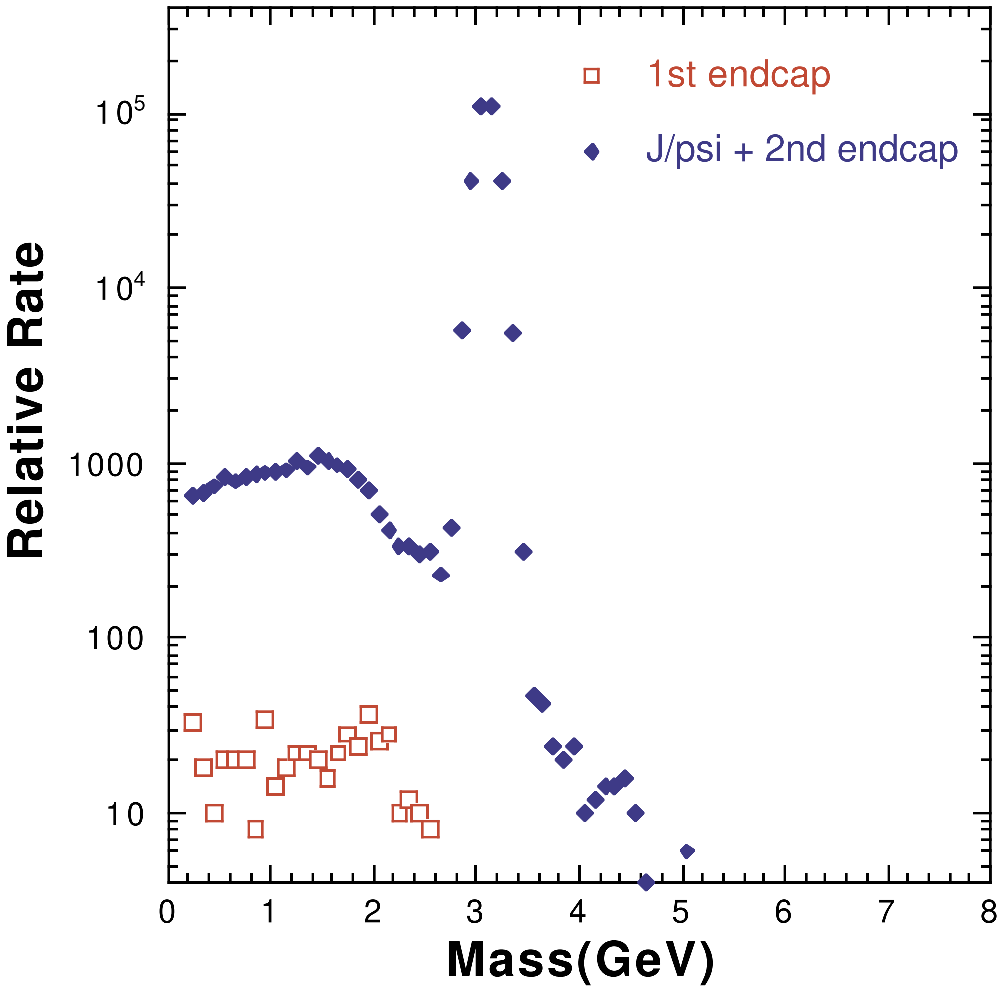

Figure 15: Simulation of J/ψ events and pion decay background at $\sqrt{s} = 50\ GeV$. The upper points are events accepted in the second muon arm with no hadron absorbing "nose cone" placed before the central magnet pole tip. The lower curve shows the corresponding decay background in the first muon arm in the configuration of the PHENIX CDR[25] (which includes the "nose cone", neutron shield, and Pb photon/electron shield). The simulations were performed with PISA[41], using pion production cross sections from Alper, *et al.* [42].

A Parton Kinematics

Collisions of partons of momenta $x_1\sqrt{s}/2$ and $-x_2\sqrt{s}/2$ in the center-of-mass system yield an intermediate state of mass M where,

$$\tau \equiv M^2/s = x_1 x_2, \tag{1}$$

and,

$$x_F \equiv x_1 - x_2. \tag{2}$$

A binary decay into massless final state particles yields,

$$tan\theta_{cm} = 2\sqrt{\tau}\ sin\theta_r/(\sqrt{x_F^2 + 4\tau}\ cos\theta_r \pm x_F), \tag{3}$$

where θ_r is the decay angle in the rest frame of the intermediate state. Thus the geometry of final-state particle detection depends only on x_F and $\sqrt{\tau}$. Considering for simplicity the case $\theta_r = \pi/2$, one finds that the opening angle between the final state particles is,

$$\theta_o = 2tan^{-1}(2\sqrt{\tau}/x_F). \tag{4}$$

B Scaling of the Drell-Yan Cross Section

The choice of colliding-beam energy for polarized DY physics is important since the cross sections are small and the region in which large polarization effects are most likely to be observed is $0.01 \leq x_{\bar{u}} \leq 0.2$. The region, $x_{\bar{u}} \geq 0.2$ is inaccessible due to the steeply falling structure function $\bar{u}(x)$. Optimization of the collision energy can be accomplished by reducing the DY cross section,

$$M^3 \frac{d^2\sigma}{dM dx_F} = \frac{8\pi\alpha^2}{9} \frac{x_1 x_2}{x_1 + x_2} \times \sum_i e_i^2 [q_i(x_1)\bar{q}_i(x_2) + \bar{q}_i(x_1) q_i(x_2)], \tag{1}$$

to the scaling form,

$$d^2\sigma / d\sqrt{\tau} dx_F \propto 1/s \times \mathcal{F}(\tau, x_F). \tag{2}$$

From Appendix A one sees that the acceptance of a spectrometer depends only on τ and x_F. This means that $A_{LL}(x_1, x_2)$ may be measured with roughly equal acceptance at $M = 4\ GeV$, $\sqrt{s} = 50\ GeV$ or $M = 16\ GeV$, $\sqrt{s} = 200\ GeV$; however, from Eq. 2 the cross section at $\sqrt{s} = 50\ GeV$ will be 16 times larger.[11]

Finally, the luminosity of RHIC for pp collisions is expected to scale as $L \propto \sqrt{s}$. Thus, the event rate,

$$R_{ev} \sim L \times \sigma_{DY}(x_1, x_2) \propto 1/\sqrt{s}. \tag{3}$$

[11] This is only an approximation since the muon energies increase with $\sqrt{s}$, and higher energy muons are generally detected with somewhat higher efficiency.

References

[1] J. Ashman et al., Phys. Lett **B206**, 364(1988); Nucl. Phys. **B328**, 1(1989).

[2] M.J. Alguard et al., Phys. Rev. Lett. **37**, 1261(1978), **41**, 70(1978); G. Baum et al., Phys. Rev. Lett. **51**, 1135(1983).

[3] R.L. Jaffe and A. Manohar, Nucl. Phys. **B337** 509(1991); and references therein.

[4] D. Adams et al., Phys. Lett. **B329**, 399(1994).

[5] B. Adeva et al., Phys. Lett. **B302**, 533(1993).

[6] P.L. Anthony et al., Phys. Rev. Lett. **71**, 959(1993).

[7] The HERMES Experiment at the Deutsches Elektronen Synchrotron (DESY), DESY World Wide Web Server home page.

[8] F.E. Close and D. Sivers, Phys. Rev. Lett. **39**, 1116(1977).

[9] J. Ralston and D.E. Soper, Nucl. Phys. **B152**, 109(1979).

[10] J. Kodaira, et al., Nucl. Phys. **B159**, 99(1979).

[11] A.P. Bukhvostov, E.A. Kuraev, and L.N. Lipatov, Zh. Eksp. Teor. Fiz **87**, 37(1984); Sov. Phys. JEPT **60**, 22(1984).

[12] X. Artru and M. Mekhfi, Z. Phys. **C 45**, 669(1990).

[13] J. Collins, Proc. of the Polarized Collider Workshop, Penn State University (1990), eds. J. Collins, S Heppelmann, and R.W. Robinett, AIP conf. proc. No. **223**, AIP New York (1991).

[14] R.L. Jaffe and Xiangdong Xi, Phys. Rev. Lett. **67**, 552(1991).

[15] G. Bunce et al., Particle World, **3**, 1(1992).

[16] RHIC Spin Collaboration, AGS/RHIC proposal, Aug. 1992; Update, Sept. 2, 1993.

[17] S.D. Drell and T-M. Yan, Phys. Rev. Lett. **25**, 316(1971).

[18] W.J. Stirling and M.R. Whalley, Journal of Phys. **G 19**, D1(1993).

[19] Claude Bourrely and Jacques Soffer, Phys. Lett. **B 314**, 132(1993).

[20] P. Amaudruz et al., Phys. Rev. Lett. **66**, 2712(1991).

[21] CERN, NA51 Collaboration, Phys. Lett. in press.

[22] K. Gottfried, Phys. Rev. Lett. **18**, 1174(1967).

[23] G. Moreno et al., Phys. Rev. **D43**, 2815(1991).

[24] D.M. Alde et al., Phys. Rev. Lett. **64**, 2479(1990); P.L. McGaughey et al., Phys. Rev. **D 50**, 3038(1994).

[25] Conceptual Design Report of the PHENIX Collaboration and updates.

[26] M. Magano et al., Nucl. Phys. **B 405**, 507(1993).

[27] Claude Bourrely and Jacques Soffer, Nucl. Phys. **B423**, 329(1994).

[28] C. Albajar et al. (UA1 Collaboration), Phys. Lett. **B 253**, 503(1991).

[29] A. Maciel et al. (D0 Collaboration), Fermilab Conf. 93/395-E (1993).

[30] F. Abe et al. (CDF Collaboration), Phys. Rev. Lett. **67**, 1502(1991).

[31] P. Chiappetta et al., Phys. Lett. **B 183**, 215(1987).

[32] E.L. Berger and J. Qiu, Phys. Rev. **D 40**, 778(1989).

[33] Z. Kunszt, Phys. Lett. **B 218**, 243(1989).

[34] G. Altarelli and W.J. Stirling, Particle World, **1**, 40(1989).

[35] J.L. Cortes and B. Pire, Phys. Rev. **D 38**, 3586(1988).

[36] M.A. Doncheski and R.W. Robinett, Phys. Lett. **B 248**, 188(1990); R.W. Robinett, Phys. Rev. **D 43** 113,(1991).

[37] A.P. Contogouris, et al., Phys. Lett. **B 246**, 523(1990); M. Karliner and R.W. Robinett, Phys. Lett. **B 324**, 209(1994).

[38] V. Barger et al., Z. Phys. **C6**, 169(1980); R. Baier and R. Rückl, Z. Phys. **C 19**, 251(1983); V.Barger and A.D. Martin, Phys. Rev. **D 31**, 1051(1985).

[39] L. Antonaizzi et al., Phys. Rev. Lett. **70**, 383(1993); and references therein.

[40] J.P Rutherfoord, AIP Conference Proceedings **176**, 157(1988).

[41] PHENIX Integrated Simulation code, based on GEANT.

[42] B. Alper et al., Nucl. Phys. **B100**, 237(1975).